Scientific Reports

https://doi.org/10.1038/s41598-026-38213-3

Article in Press

PERK inhibition attenuates multi-program cell death through Nrf2/HO-1 activation in diabetic retinopathy with integrated proteomics and functional validation in HRECs

Received: 9 August 2025

Accepted: 29 January 2026

Published online: 04 February 2026

Cite this article as: Xie L., Zhang X., Tian M. *et al.* PERK inhibition attenuates multi-program cell death through Nrf2/HO-1 activation in diabetic retinopathy with integrated proteomics and functional validation in HRECs. *Sci Rep* (2026). https://doi.org/10.1038/s41598-026-38213-3

Like Xie, Xinran Zhang, Min Tian, Min Tang, Qi Zhou & Hongbin Lv

PERK Inhibition Attenuates Multi-Program Cell Death through Nrf2/HO-1 Activation in Diabetic Retinopathy with Integrated Proteomics and Functional Validation in HRECs

Like Xie[1#], Xinran Zhang[1#], Min Tian[2], Min Tang[3], Qi Zhou[✉], Hongbin Lv[✉]

[1, 2, 3]Department of Ophthalmology, The Affiliated Hospital of Southwest Medical University, Luzhou, Sichuan, 646000, P.R. China.

✉Corresponding Author:Qi Zhou , Department of Ophthalmology, The Affiliated Hospital of Southwest Medical University, No. 25 Taiping Street, Jiangyang District, Luzhou 646000, Sichuan Province, P.R. China.

email:113454771@qq.com; Hongbin Lv DR, Department of Ophthalmology, The Affiliated Hospital of Southwest Medical University, No. 25 Taiping Street, Jiangyang District, Luzhou 646000, Sichuan Province, P.R. China.

email:oculistlvhongbin@163.com

[#] Contributed equally.

Abstract

Objective: To investigate whether protein kinase R-like ER kinase (PERK) inhibition mitigates hyperglycemia (HG)-induced multi-modal cell death, including ferroptosis, apoptosis, and pyroptosis, in human retinal endothelial cells (RECs) (HRECs) through activation of the nuclear factor erythroid 2-related factor 2 (Nrf2)/heme oxygenase-1 (HO-1) pathway, thereby providing a unified therapeutic strategy for diabetic retinopathy.

Methods: HRECs were cultured in normal glucose (NG, 5.5 mM, 48 h) and HG (HG, 25 mM, 48 h) DMEM media, with or without the PERK inhibitor ISRIB or the ferroptosis inhibitor Fer-1. Protein

expression profiles from NG and HG-treated cells were compared using tandem mass tag (TMT)-LC-MS/MS and subjected to bioinformatic analysis. Cell viability was assessed via CCK-8 assay. Ferroptosis markers (Malondialdehyde (MDA), reactive oxygen species (ROS), Fe^{2+}, GSH, glutathione peroxidase 4 (GPX4)), apoptosis mediators (caspase-3, caspase-7, Bcl-2), and pyroptosis markers (NLRP3, caspase-1, gasdermin D (GSDMD)) were quantified through biochemical assays and ELISA. Expression levels of PERK, Nrf2, and HO-1 were analyzed by real-time quantitative PCR (RT-qPCR) and Western blotting.

Results: Proteomic analysis identified 247 differentially expressed proteins (DEPs) significantly enriched in ferroptosis and peroxisome proliferator-activated receptor (PPAR) signaling pathways. HG conditions induced concurrent ferroptosis (increased MDA, ROS, Fe^{2+}; decreased ↓GSH, GPX4), apoptosis (elevated caspase-3 and caspase-7; reduced ↓Bcl-2), and pyroptosis (upregulated NLRP3, caspase-1, and GSDMD; all $p < 0.001$). Treatment with ISRIB reversed these effects by normalizing ferroptosis markers, suppressing apoptosis (reduced caspase-3 and caspase-7; increased ↑Bcl-2), and inhibiting pyroptosis (decreased ↓NLRP3, caspase-1, GSDMD). Mechanistically, ISRIB activated the Nrf2/HO-1 pathway while downregulating PERK, with no significant effects observed under normoglycemic conditions.

Conclusion: PERK inhibition simultaneously attenuates HG-induced ferroptosis, apoptosis, and pyroptosis in HRECs via activation of the Nrf2/HO-1 pathway. This coordinated blockade presents a promising therapeutic strategy to preserve retinal vasculature in diabetic retinopathy.

Keywords: diabetic retinopathy; protein kinase R-like ER kinase; nuclear factor erythroid 2-related factor 2; ferroptosis; apoptosis; pyroptosis; human retinal endothelial cells; endoplasmic reticulum stress.

1. Introduction

Diabetic retinopathy (DR), a microvascular complication affecting over 140 million individuals worldwide, remains a leading cause of visual impairment and blindness despite advances in glycemic control [1]. The early stages of DR are marked by the loss of retinal endothelial cells (RECs) and the consequent disruption of the blood-retinal barrier [2, 3]. Although apoptosis has traditionally been considered a primary mechanism underlying REC loss, accumulating evidence indicates that the spectrum of cell death modalities involved in DR is more complex and incompletely understood [4].

Recent studies have increasingly implicated non-apoptotic cell death pathways in the pathogenesis of diabetic complications. Ferroptosis, an iron-dependent form of regulated cell death characterized by unchecked lipid peroxidation, has emerged as a critical contributor [5-7]. However, its precise role and regulation within human RECs (HRECs) under hyperglycemic stress remain poorly defined. Simultaneously, hyperglycemia (HG)-induced endoplasmic reticulum (ER) stress activates the protein kinase R-like ER kinase (PERK) pathway, a key mediator of cellular stress responses that may coordinate crosstalk among diverse cell death programs [8-10]. The transcription factor nuclear factor erythroid 2-related factor 2 (Nrf2) and its downstream effector heme oxygenase-1 (HO-1) constitute a pivotal cytoprotective axis against oxidative damage, yet the interplay between Nrf2/HO-1 signaling

and PERK in diabetic RECs remains to be fully elucidated [11-13]. Proteomic analyses in DR models have revealed dysregulation of multiple pathways, including peroxisome proliferator-activated receptor (PPAR) signaling, suggesting multifactorial control of cell death mechanisms [14-16]. Notably, emerging data indicate that ferroptosis, apoptosis, and pyroptosis may converge via shared molecular mediators, such as caspase-3, gasdermin D (GSDMD), and reactive oxygen species (ROS), engaging in positive feedback loops that amplify cellular demise [17-19].

Despite these advances, a significant knowledge gap persists: a comprehensive and integrated understanding of how PERK signaling orchestrates multiple concurrent cell death pathways in human RECs is lacking [20]. Current research is limited by an overreliance on rodent models that differ substantially from humans in redox regulation [21, 22], incomplete characterization of the ER stress-ferroptosis axis [23], and the largely unexplored therapeutic potential of targeting PERK in human DR [24].

To address these gaps, we designed a study integrating tandem mass tag (TMT) quantitative proteomics with functional validation in HG stressed HRECs. We hypothesized that PERK inhibition attenuates HG-induced multi-program cell death, including ferroptosis, apoptosis, and pyroptosis, via activation of the Nrf2/HO-1 axis. To test this hypothesis, we first performed unbiased proteomic profiling to map global protein expression changes and identify key enriched pathways. Subsequently, we pharmacologically inhibited PERK using ISRIB, a potent and selective PERK inhibitor, to functionally validate its regulatory role across the three cell death modalities. The inclusion of Fer-1, a ferroptosis-specific inhibitor, further allowed us to delineate

ferroptosis' specific contribution within the broader cell death network. This integrated approach aims to establish PERK as a central regulatory node coordinating convergent death pathways in DR and to evaluate its potential as a novel therapeutic target for preserving retinal vasculature integrity.

2 Materials and Methods

2.1 Cell culture

HRECs were obtained from Beina Bio-Tech Co., Ltd. (China) and cultured in a humidified incubator at 37°C with 5% CO_2. Cells were maintained in a fully supplemented culture medium composed of DMEM, fetal bovine serum, and an antibiotic mixture in a ratio of 89:10:1. For experiments, HRECs were cultured in either (NG; 5.5 mM, 48 h) or (HG; 25 mM, 48 h) DMEM media, with or without the PERK inhibitor ISRIB (10 μM) or the ferroptosis inhibitor Ferrostatin-1 (Fer-1; 1 μM). The DMEM media used for NG and HG conditions contained the respective glucose concentrations without additional D-glucose supplementation.

2.2 CCK-8 cell viability assay

We initially assessed cell viability at 24, 48, and 72 hours to determine the optimal duration of HG exposure. Subsequently, cells were grouped as described in Section 2.1 for the definitive viability assay. Cells were harvested by trypsin digestion, which was terminated by adding fully supplemented culture medium to obtain a single-cell suspension. A suspension containing 5.0×10^4 cells/mL was prepared, and 100 μL (equivalent to 5,000 cells) was seeded into each well of a 96-well plate. The plate was incubated at 37°C with 5% CO_2 until the cells adhered to the well bottom. Next, 10 μL of CCK-8 reagent was added to each well, and the plate was incubated in the dark for 90 minutes. Finally, absorbance was

measured at 450 nm to quantify cell viability.

2.3 Proteomics of HG-induced HRECs

2.3.1 Protein extraction and enzymatic digestion

HRECs were cultured in NG DMEM medium (NG, 5.5 mM, 48 h) and HG DMEM medium (HG, 25 mM, 48 h) without the addition of the PERK inhibitor ISRIB (10 μM) or the ferroptosis inhibitor Fer-1 (1 μM). Cells were lysed using SDT lysis buffer and subjected to ultrasonic fragmentation on ice. The lysates were then boiled in a water bath for 15 minutes, followed by centrifugation at 14,000 × g for 15 minutes at 15°C. The supernatant was collected for subsequent analysis. Protein concentration was determined using a bicinchoninic acid (BCA) assay kit. For each sample, 200 μg of protein solution was taken, and DTT was added to a final concentration of 100 mM, followed by incubation in a water bath for 5 minutes. Next, 200 μL of UA buffer was added, mixed thoroughly, and transferred to a 30 kDa ultrafiltration tube. The sample was centrifuged at 12,500 × g for 25 minutes, and the filtrate discarded. Subsequently, 100 μL of IAA buffer was added, and the mixture was shaken at 600 rpm for 1 minute, then incubated at room temperature in the dark for 30 minutes. After incubation, the sample was centrifuged again at 12,500 × g for 25 minutes. Following this, 100 μL of UA buffer was added and centrifuged at 12,500 × g for 15 minutes. Then, 100 μL of 0.1 M TEAB solution was added, and the sample was centrifuged at 12,500 × g for 15 minutes. Next, 40 μL of trypsin solution was added, mixed by shaking at 600 rpm for 1 minute, and incubated at 37°C for 16-18 hours. After digestion, the collection tube was replaced with a new one, and the sample was centrifuged at 12,500 × g for 15 minutes. Finally, 20 μL of 0.1 M TEAB solution was added, followed by a final centrifugation at 12,500 × g for 15 minutes to collect the filtrate.

2.3.2 Mass spectrometry identification

Samples were chromatographically separated and analyzed using a Q Exactive Plus mass spectrometer. The analysis duration was 60 to 90 minutes, with detection performed in positive ion mode. Full MS scans were acquired over an m/z range of 350-1800, at a resolution of 70,000, with an automatic gain control (AGC) target of 3×10^6 and a maximum injection time (IT) of 50 ms. Following each full scan, 10 fragmentation spectra (MS2 scans) were collected.

2.3.3 Data analysis

Quantitative proteomics analysis was conducted using the Q Exactive Plus mass spectrometer. The raw data files (.raw) were converted to .mgf format using Proteome Discoverer 2.2 software and subsequently submitted to the MASCOT 2.6 server for database searching against the UniProt_HomoSapiens_20394_20210127 database. The resulting database search files (.dat) were imported back into Proteome Discoverer 2.2, and data filtering was performed based on a false discovery rate (FDR) threshold of less than 1% (FDR < 0.01) to ensure high-confidence qualitative results.

2.3.4 Bioinformatics analysis

Specific bioinformatics analyses, including gene ontology (GO) analysis (http://geneontology.org/) and Kyoto encyclopedia of genes and genomes (KEGG) pathway analysis (https://www.kegg.jp/), were performed on all differentially expressed proteins (DEPs) using Blast2GO software. Significant pathway enrichment was determined using Fisher's exact test, which assesses the association between the number of DEPs and the total number of proteins annotated to each pathway.

2.4 Study on the Mechanism of HG-Induced Ferroptosis in HRECs

2.4.1 Malondialdehyde (MDA) and superoxide dismutase (SOD) detection

Cell culture and grouping were performed as described in Section 2.1.

SOD activity was measured using the SOD Detection Kit (Kit A001-3, Jiancheng, Nanjing, China), based on the WST-1 method. Briefly, 20 μL of sample, 20 μL of enzyme working solution, and 200 μL of substrate solution were thoroughly mixed in a test tube and incubated for 30 minutes. Absorbance was then measured at 450 nm, and the SOD inhibition rate was calculated according to the kit's formula.

MDA levels were determined using the MDA Detection Kit (Kit A003-1, Jiancheng, Nanjing, China), based on the thiobarbituric acid (TBA) method. Harvested cells were lysed, and the supernatant collected after centrifugation. The lysate was reacted with TBA solution at 95°C for 30 minutes. After cooling and centrifugation, the absorbance of the supernatant was measured at 532 nm. MDA concentration was calculated by comparing sample absorbance with a concurrently run MDA standard curve, and results were normalized to total protein content and expressed as nmol/mL protein.

2.4.2 Lipid peroxide detection

Cell culture and grouping were performed as described in Section 2.1. Intracellular lipid peroxidation was evaluated using the Liperfluo probe (Dojindo, L248, Shanghai, China). After 36 hours of initial culture, cells were seeded into confocal dishes and further incubated for 12 hours. The cells were then thoroughly washed with phosphate-buffered saline (PBS), and the culture medium was removed. Liperfluo solutions at concentrations of 10 μM, 20 μM, and 30 μM were prepared in serum-free DMEM and added to the dishes,

followed by incubation for 40 minutes in a cell culture incubator. After incubation, the probe solution was removed, and the cells were washed thoroughly with HBSS. Fluorescence imaging was performed using laser confocal microscopy with excitation and emission wavelengths set at 488 nm and 500-550 nm, respectively.

2.4.3 ROS and Fe^{2+} detection

Cell culture and grouping were performed as described in Section 2.1.

ROS levels were measured using the ROS Assay Kit (Jiancheng, E004-1-1, Nanjing, China) following the manufacturer's instructions. Briefly, cells were incubated with the DCFH-DA probe diluted in serum-free culture medium at 37°C for 20 minutes. After incubation, cells were collected into 1.5 mL centrifuge tubes and washed with PBS to remove excess probe. The cells were then centrifuged at 1,000 × g for 5 minutes, the supernatant discarded, and the pellet resuspended in PBS for fluorescence measurement. The assay was performed with an excitation wavelength of 488 nm and an emission wavelength of 525 nm.

Intracellular Fe^{2+} levels were determined using the Fe^{2+} Assay Kit (Solarbio, BC5414, Beijing, China). Approximately 5×10^6 cells were resuspended in 1 mL of assay solution 1 and sonicated on ice to lyse the cells. The lysate was centrifuged at 10,000 × g for 10 minutes at 4°C. The spectrophotometer or ELISA reader was preheated for at least 30 minutes and set to measure absorbance at 593 nm. Test, standard, and blank samples (200 μL each) were prepared in 1.5 mL centrifuge tubes, and the supernatants were transferred to micro glass colorimetric cuvettes or 96-well plates for absorbance measurement at 593 nm.

2.4.4 Glutathione peroxidase 4 (GPX4) and GSH detection

Cell culture and grouping were performed as described in

Section 2.1.

GPX4 levels were measured using an ELISA kit (ELK Biotechnology, ELK4775, Wuhan, China). Cells were lysed by ultrasonic disruption, and 100 µL of either working buffer or sample was added to each well, followed by incubation at 37°C for 80 minutes. After three washes, wells were incubated with 100 µL of antibody solution at 37°C for 50 minutes. Subsequently, 100 µL of working solution was added for a further 50-minute incubation. The plate was then incubated in the dark for 20 minutes after adding the TMB substrate. Finally, the reaction was stopped with stop buffer, and the optical density (OD) was measured at 450 nm using a plate reader with 1-minute shaking.

Glutathione (GSH) levels were quantified using the GSH assay kit (Jiancheng, A006-1, Nanjing, China). Cells were resuspended in PBS and transferred into 1.5 mL centrifuge tubes. After centrifugation at 1,000 × g for 5 minutes, the supernatant was discarded, and cells were resuspended in PBS. Two milliliters of assay reagent 1 was added and mixed thoroughly, followed by centrifugation at 3,500-4,000 × g for 10 minutes. One milliliter of the resulting supernatant was used for the colorimetric assay. Blank, standard, and test tubes were prepared according to the manufacturer's instructions. After thorough mixing, samples were allowed to react for 5 minutes. Absorbance was measured at 420 nm using a spectrophotometer with a 1 cm light path.

2.4.5 qPCR and Western blot detection of pathway key factor expression

Cell culture and grouping were performed as described in Section 2.1. Total RNA was extracted from cultured cells using TRIzol reagent (Invitrogen) following the manufacturer's protocol. Briefly, cells were lysed directly in the culture dish with TRIzol. After

adding chloroform and centrifuging for phase separation, the aqueous phase containing RNA was carefully collected. RNA was precipitated with isopropanol, washed with 75% ethanol, and dissolved in RNase-free water. RNA concentration and purity were assessed using a NanoDrop spectrophotometer. Complementary DNA (cDNA) was synthesized from extracted RNA using the reverse transcription kit from Toyobo (Fsq-201, Shanghai, China) according to the manufacturer's instructions. Real-time quantitative PCR (RT-qPCR) was performed with the following primer sequences: Nrf2 forward: GGTTGCCCACATTCCCAAATC, Nrf2 reverse: CAAGTGACTGAAACGTAGCCG; HO-1 forward: TTCAAGCAGCTCTACCGCTC, HO-1 reverse: GAACGCAGTCTTGGCCTCTT; with GAPDH (Forwad:TGACATCAAGAAGGTGGTGAGCAG, reverse:GTGTCGCTGTTGAAGTCAGAGGAG) as an internal reference gene, and the $2-\Delta\Delta Ct$ method was used for data analysis.

Protein extraction and quantification: Total protein was extracted from adherent cells following this procedure. Cells were rinsed twice with ice-cold PBS, and residual liquid was carefully aspirated after the final wash. An appropriate volume of ice-cold lysis buffer, freshly supplemented with 1× protease inhibitor cocktail, was added to the culture plate or flask. For proteins susceptible to degradation or present at low abundance, specific phosphatase inhibitors or other relevant enzyme inhibitors were also included. Cells were lysed at room temperature for 3-5 minutes with gentle rocking to ensure thorough exposure to the lysis buffer. The cell lysate was then scraped using a cell scraper and transferred to a pre-chilled 1.5 mL microcentrifuge tube. The lysate was incubated on ice for 30 minutes, with intermittent pipetting to enhance lysis. Subsequently, samples were centrifuged at 12,000 × g for 5 minutes

at 4°C. The resulting supernatant containing total protein was collected and stored at -80°C until further analysis. Protein concentration was measured using the BCA protein assay kit (ASPEN Biological, AS1086, Wuhan, China). Equal amounts of protein were separated by SDS-PAGE according to molecular weight and then transferred onto nitrocellulose membranes. Membranes were incubated with the appropriate primary and secondary antibodies. Detection was performed using the ECL chemiluminescence kit (ASPEN Biological, AS1059, Wuhan, China). Freshly prepared ECL solution was applied to the membrane's protein side, and signals were captured under darkroom conditions.

2.5 Statistical analysis

All statistical analyses were performed using SPSS (version 26.0), and graphical representations were generated with GraphPad Prism (version 10.0). For functional enrichment analyses (GO and KEGG), p-values were adjusted for multiple comparisons using the FDR method, with an FDR threshold of < 0.01 considered statistically significant. Experiments were conducted in triplicate, with three independent samples per group ($n = 3$). Data distribution and homogeneity of variance were assessed using the Shapiro-Wilk test and appropriate variance tests before further analysis. Parametric data are presented as means ± standard deviations (SD) and analyzed by one-way ANOVA followed by Dunnett's multiple comparisons test. Non-parametric data are expressed as medians with interquartile ranges [M (IQR)] and analyzed using the Kruskal-Wallis test with suitable post-hoc comparisons. A two-tailed p-value < 0.05 was considered statistically significant. Key results are reported with 95% confidence intervals.

3 Result

3.1 DEPs analysis

A total of 6,662 proteins were identified, among which 247 were DEPs (Fig. 1A-B). Of these DEPs, 90 were significantly upregulated and 157 significantly downregulated in the HG group compared to the NG group. Notably, the upregulated DEPs included TGFB1, AMER2, and other proteins closely associated with the Wnt signaling pathway and ferroptosis (Fig. 1C). Conversely, downregulated DEPs included AFP, ZFAND2A, and proteins implicated in diabetic nephropathy and the NF-κB signaling pathway (Fig. 1D).

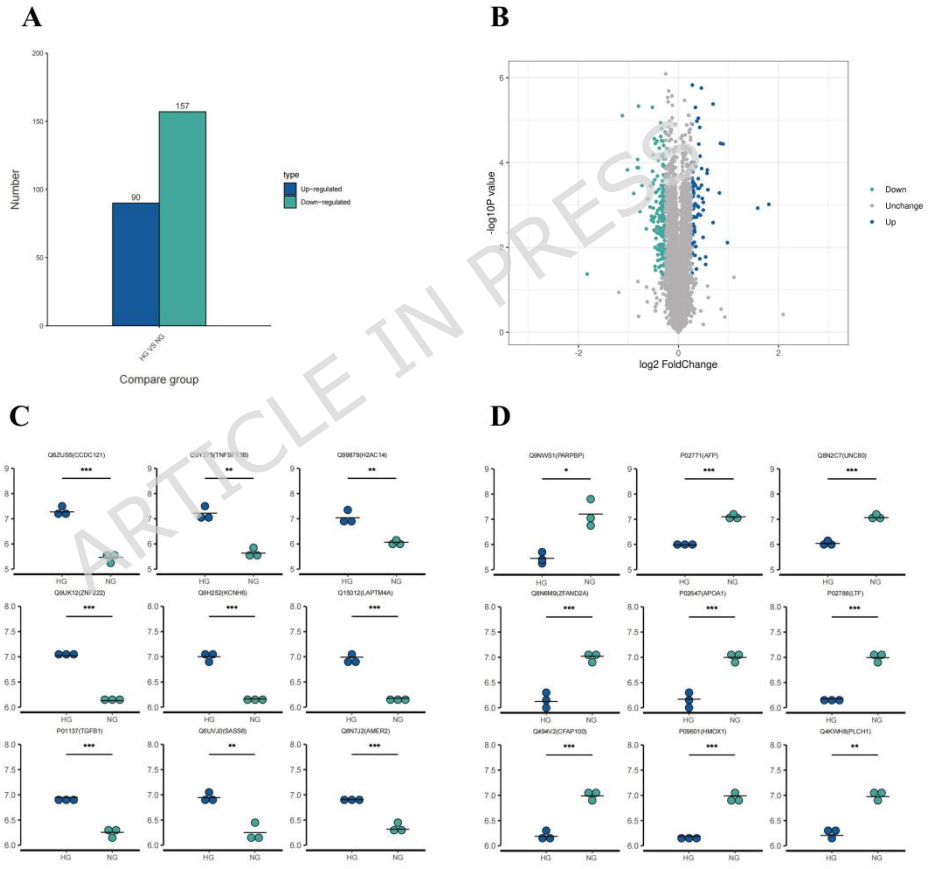

Fig. 1. DEPs analysis (A) The bar chart shows the number of DEPs that differ between groups. (B) The results of differential protein screening are presented in the form of volcano plot. (C) The scatter plot shows the upregulated proteins. (D) The scatter plot shows downregulated proteins. *p*-value 0.05. n=3.

3.2 GO Enrichment Analysis Reveals HG-Induced Pathogenic Mechanisms in HRECs

Based on GO enrichment analysis (Fig. 2A), upregulated and downregulated proteins showed distinct distributions across biological processes, molecular functions, and cellular components. Upregulated proteins were primarily involved in stress-response mechanisms, while downregulated proteins were associated with the suppression of normal physiological functions. This coordinated functional shift, reflected in specific subcellular localizations, contributes to the observed disease phenotype. GO functional annotation revealed that DPEs in HG-stressed RECs were significantly enriched in fundamental functional categories. The most prominent biological processes included "cellular process," "biological regulation," and "metabolic process," with enrichment of "response to stimulus" confirming activation of stress response pathways (Fig. 2B). Molecular functions were predominantly "binding" and "catalytic activity," indicating alterations in molecular interactions and enzymatic functions (Fig. 2C). Cellular component analysis demonstrated that affected proteins localized mainly to the "cell part," "organelle part," and "protein-containing complex," suggesting that HG primarily impacts core cellular structures and macromolecular assemblies (Fig. 2D). Together, these findings illustrate extensive cellular remodeling under diabetic conditions.

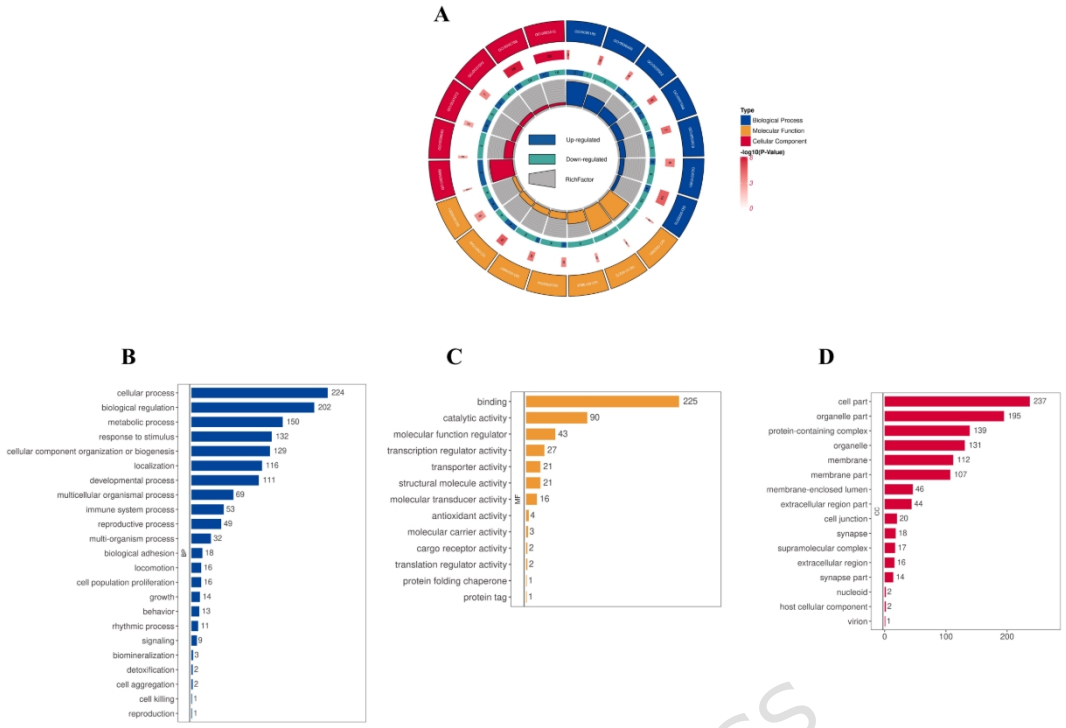

Fig.2.GO Enrichment Analysis Reveals HG induced-Induced Pathogenic Mechanisms in HRECs. (A) The circos plot depicts the top 20 most significantly enriched GO terms. (B-D) The bar chart shows the number of differential DEPs at the level of GO secondary functional annotation. p-value 0.05.

3.3 KEGG Enrichment Analysis Reveals HG induced-Induced Pathogenic Mechanisms in HRECs

KEGG pathway analysis revealed significant enrichment in neurodegenerative pathways, proteotoxic and ER stress responses, as well as dysregulated survival signaling pathways including PI3K-Akt and various cancer-related pathways. These findings indicate a simultaneous disruption of protein homeostasis and the balance between cell death and survival. Additionally, co-enrichment of pathways related to atherosclerosis and viral infection underscores a pathological state characterized by intensified inflammation and cellular stress, collectively contributing to disease progression (Fig. 3A).

Further KEGG enrichment analysis of DEPs in HG-stressed HRECs highlighted several significantly enriched pathways, with a prominent focus on ferroptosis and associated stress responses (Fig. 3B). Ferroptosis emerged as the most significantly enriched pathway, strongly implicating this iron-dependent, lipid peroxidation-driven form of regulated cell death as a key mechanism underlying HG-induced cytotoxicity. This is corroborated by the concurrent enrichment of the Mineral absorption pathway, essential for cellular iron homeostasis, and the PPAR signaling pathway, a critical regulator of lipid metabolism and oxidative stress. The co-enrichment of these pathways suggests coordinated dysregulation of iron metabolism and lipid peroxidation, fundamental biochemical events in ferroptosis.

Moreover, enrichment of pathways such as Fluid shear stress and atherosclerosis, along with several cancer-related pathways (e.g., bladder cancer, hepatocellular carcinoma), which involve oxidative stress, apoptosis, and inflammation, implies that ferroptosis likely operates in concert with other cell death and stress-response mechanisms, collectively driving REC loss. The identification of the Drug metabolism - other enzymes pathway further suggests additional sources of oxidative stress in this context. Altogether, these proteomic findings support a comprehensive model in which HG stress initiates a multifaceted cell death response in HRECs, with ferroptosis acting as a central, oxidative stress-sensitive hub.

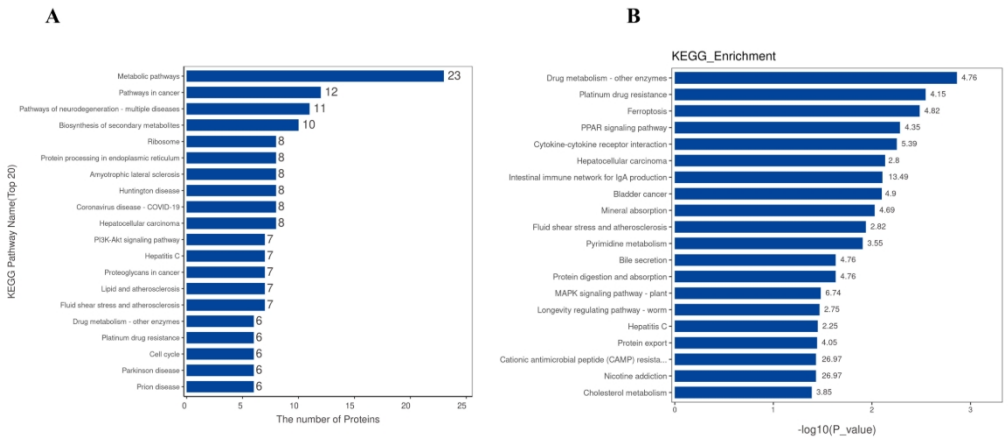

Fig. 3.KEGG Enrichment Analysis Reveals HG induced-Induced Pathogenic Mechanisms in HRECs. (A) The bar chart shows the annotation results of the top 20 KEGG pathways, the number on the right shows the difference in DEPs.(B) The bubble diagram shows the information of the top 20 enriched pathways in the result of KEGG enrichment analysis, the number on the right represents the RichFactor value. *p*-value 0.05.

3.4 The optimal intervention time for HG and changes in cell proliferation activity after intervention

Figure 4A shows that cell viability in the HG group was significantly reduced at 48 hours, indicating that 48 hours is an optimal duration for HG exposure.

As shown in Figure 4B, cell proliferation was markedly decreased in the HG group compared to the NG control. Although proliferation in the HG + Fer-1 and HG + ISRIB groups was also reduced relative to the normoglycemic group, both treatments significantly improved proliferation compared to the HG group alone. These results suggest that HG inhibits cell proliferation, while treatment with Fer-1 or ISRIB partially reverses this inhibitory effect.

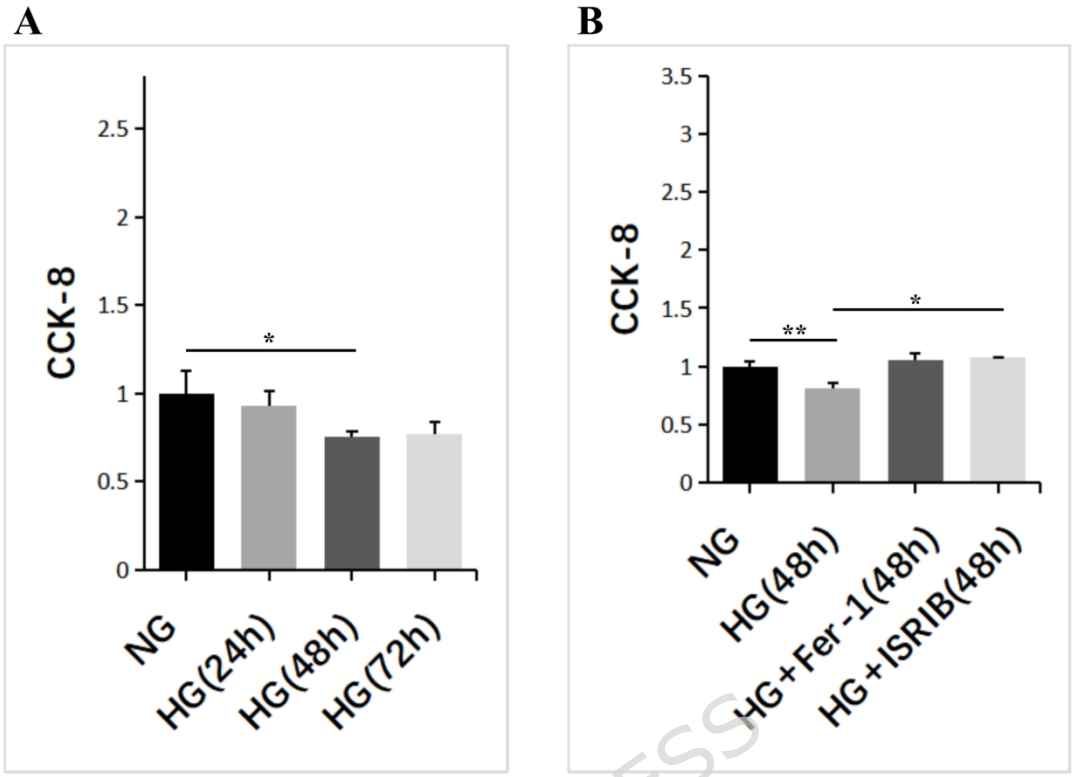

Fig. 4. The optimal intervention timing for HG-induced changes in HRECs proliferation and the influence of Fer-1 and ISRIB on the proliferative activity of HRECs induced by HG. (A) Proliferative activity of HRECs induced by HG at different time points. (B) Effects of Fer-1 and ISRIB on the HG-induced proliferative activity.Data are shown as the mean ± SEM; *$p < 0.05$, **$p < 0.01$, ***$p < 0.001$.n=3.

3.5 Detection of MDA, SOD, ROS, Fe2+, GPX4, GSH and Lipid Peroxide Levels

In lipid peroxide detection, treatment with Fer-1 or ISRIB led to increased fluorescence intensity compared to NG controls, but significantly reduced intensity relative to the HG group (Fig. 5A, 5B). The MDA concentration was markedly elevated in the HG group compared to normoglycemic controls, while both Fer-1 and ISRIB treatments significantly lowered MDA levels (Fig. 5C). Conversely, the SOD inhibition rate decreased in the HG group but increased

following Fer-1 or ISRIB intervention (Fig. 5D).

As a critical trigger of ferroptosis, ROS levels were higher in the HG group than in controls. ISRIB treatment notably reduced ROS levels compared to the untreated HG group (Fig. 5E). Cellular Fe^{2+} levels, strongly linked to ferroptosis, were elevated in HG conditions but decreased after Fer-1 treatment (Fig. 5F).

GPX4, a central inhibitor of ferroptosis, was reduced in the HG group compared to controls. Both Fer-1 and ISRIB treatments restored GPX4 levels significantly (Fig. 5G). Since GPX4 activity depends on GSH generated via the cysteine-glutamate antiporter SLC7A11, GSH levels were also measured. The HG group exhibited markedly lower GSH levels than controls, while Fer-1 and ISRIB treatments increased GSH compared to the HG group (Fig. 5H).

These findings suggest that HG exposure promotes ferroptosis by increasing pro-ferroptotic factors and decreasing protective factors, whereas PERK inhibition via ISRIB counteracts these effects, highlighting its therapeutic potential.

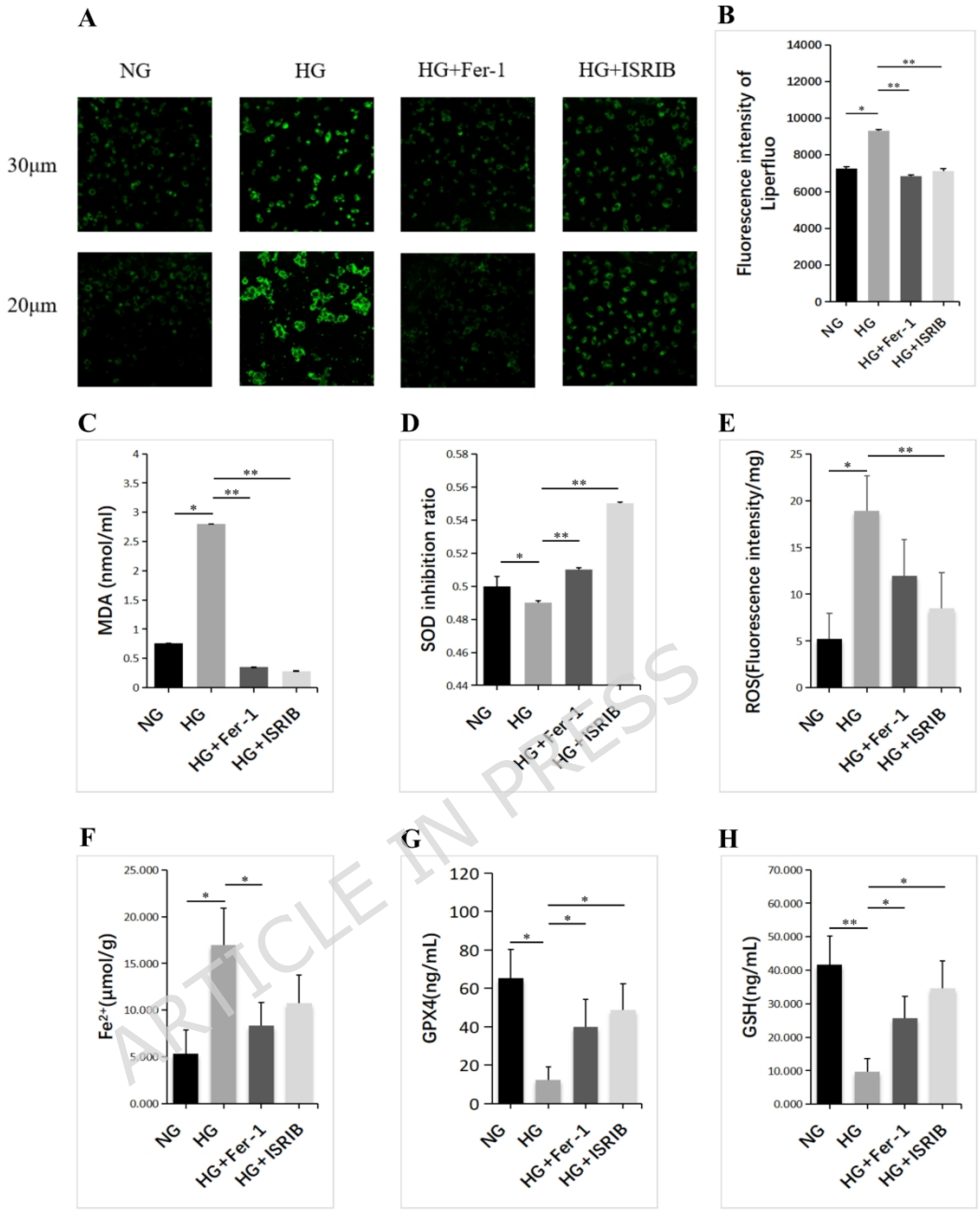

Fig. 5.Detection of MDA, SOD, ROS, Fe2+, GPX4, GSH and lipid peroxide levels. (A) Liperfluo staining visualized intracellular lipid peroxide levels.Scale bar: 125μm. (B) Fluorescence intensity quantification of lipid peroxide levels. (C, D, F, G and H) Biochemical detection of MDA, Fe^{2+}, GPX4, ROS concentration in each cell group; (E) Biochemical detection of SOD inhibition rate in each cell group; Data are shown as the mean ± SEM; *$p < 0.05$, **$p < 0.01$, ***$p < 0.001$.n=3.

3.6 RT-qPCR and Western blot detection of key factors in the PERK/Nrf2/HO-1 pathway

The HG group showed significantly suppressed Nrf2 mRNA expression compared to the normoglycemic group, while the HG + Fer-1 group did not differ significantly from the normoglycemic controls. Notably, the HG + ISRIB group exhibited markedly increased Nrf2 expression relative to the HG group (Fig. 6A). Similarly, HO-1 mRNA expression was reduced in the HG group compared to normoglycemic cells. No significant difference was observed between the HG + Fer-1 and normoglycemic groups. In contrast, the HG + ISRIB group demonstrated substantially elevated HO-1 expression compared to the HG group (Fig. 6B).

At the protein level, key components of the PERK/Nrf2/HO-1 signaling pathway displayed significant variations across groups (Fig. 6C). Both the HG and HG + Fer-1 groups showed a significant increase in PERK protein expression relative to the normoglycemic group, whereas PERK expression was markedly reduced in the HG + ISRIB group compared to both HG and HG + Fer-1 groups (Fig. 6D). Nrf2 protein levels were significantly lower in all HG-exposed groups, including the intervention groups, compared to the normoglycemic group. Moreover, Nrf2 expression in the HG + ISRIB group was significantly lower than in the HG and HG + Fer-1 groups (Fig. 6E). Finally, HO-1 protein expression was significantly decreased in all HG-treated groups relative to normoglycemic controls, with the HG + ISRIB group showing a further reduction compared to both the HG and HG + Fer-1 groups (Fig. 6F).

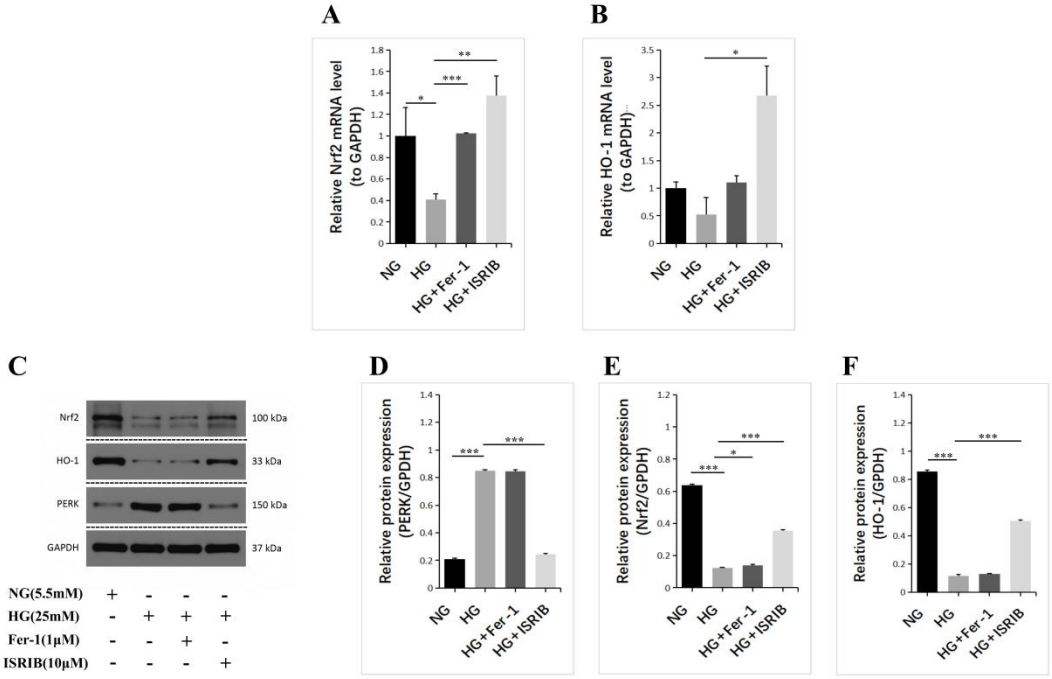

Fig. 6.RT-qPCR and Western blot detection of key factors in the PERK/Nrf2/HO-1 pathway. (A-B) mRNA expression levels of Nrf2 and HO-1 in cells from different groups; (C) Western blot analysis of Nrf2, HO-1, PERK, and GAPDH. (D-F) the relative protein expression levels of PERK, Nrf2 and HO-1 in cells from different groups. Data are shown as the mean ± SEM; *$p < 0.05$, **$p < 0.01$, ***$p < 0.001$.n=3.

3.7 ISRIB Attenuates HG-Induced Apoptotic and Pyroptotic Activation in HRECs

ELISA analysis demonstrated that HG exposure significantly activated pyroptotic signaling, as evidenced by the upregulation of NLRP3, caspase-1, and GSDMD (Fig. 7A, B, C). In contrast, treatment with ISRIB markedly suppressed these pyroptosis markers. Simultaneously, HG significantly increased pro-apoptotic mediators caspase-3 and caspase-7, while downregulating the anti-apoptotic protein Bcl-2 compared to the NG control, indicating activation of the apoptotic pathway. Notably, ISRIB co-treatment

substantially reversed these changes by reducing caspase-3 and caspase-7 levels and increasing Bcl-2 expression (Fig. 7D, E, F). Importantly, ISRIB treatment under NG conditions did not produce significant effects on any measured markers, confirming its selective efficacy in pathological, hyperglycemic settings.

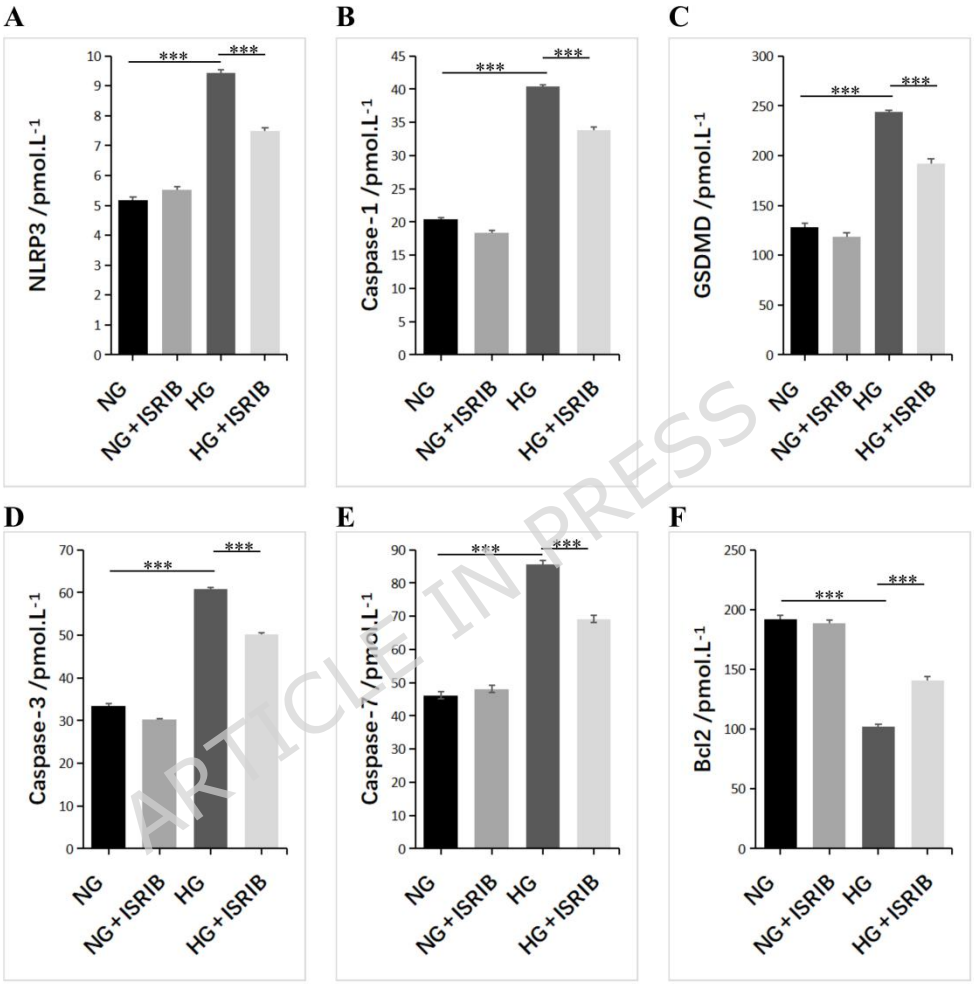

Fig. 7.ISRIB Attenuates High glucose-Induced Apoptotic and Pyroptotic Activation in Retinal Endothelial Cells. (A-C): NLRP3, Caspase-1 and GSDMD ELISA quantification. (D-F): Csapase-3, Caspase-7 and Bcl2 ELISA quantification.Data are shown as the mean ± SEM; *$p < 0.05$, **$p < 0.01$, ***$p < 0.001$.n=3.

4 Discussion

The pathogenesis of DR increasingly involves multiple

interconnected cell death pathways beyond classical apoptosis [25]. Our study provides novel evidence that HG simultaneously activates ferroptosis, apoptosis, and pyroptosis in HRECs [26]. Importantly, we demonstrate that pharmacological modulation of the Integrated Stress Response (ISR) via ISRIB, an activator of the eIF2B guanine nucleotide exchange factor, effectively attenuates all three death programs. This protective effect is mechanistically linked to restoration of the antioxidant Nrf2/HO-1 axis.

Our integrated approach, beginning with TMT-based proteomics, provided an unbiased map of HG-induced cellular perturbations. The identification of 247 DEPs and significant enrichment of ferroptosis and PPAR signaling pathways (via KEGG analysis [27, 28]) strongly implicate lipid metabolic dysregulation and oxidative stress as central mediators. These findings corroborate prior proteomic studies in diabetic retinas [29] but extend them by highlighting specific effectors such as ACSL4 and LPCAT3, which drive membrane phospholipid peroxidation, a process implicated in diabetic renal complications. We also observed significant downregulation of mitochondrial fusion proteins OPA1 and MFN2, consistent with models where mitochondrial fission promotes ferroptosis through iron-dependent lipid peroxidation [30]. Unexpected enrichment of the Hepatitis C pathway suggests viral-response mimicry, possibly via mitochondrial DNA release activating the cGAS-STING innate immunity axis, a mechanism documented in hyperglycemic and diabetic nephropathy models [31, 32] but less studied in DR. Our functional experiments validated these proteomic predictions: HG robustly induced hallmark features of ferroptosis (lipid ROS accumulation, GSH depletion, GPX4 downregulation) alongside activation of apoptotic (caspase-3/7) and pyroptotic (NLRP3, caspase-1, GSDMD) mediators. Critically, ISRIB

co-treatment concurrently mitigated all these indicators.

The mechanism of ISRIB's efficacy appears linked to the Nrf2/HO-1 axis. HG suppressed Nrf2 and HO-1 expression, effects reversed by ISRIB. This aligns with evidence that PERK can phosphorylate Nrf2 to repress antioxidant responses in endothelial cells [33], contrasting with its activating role in neurons [34], highlighting tissue-specific regulation. However, a key limitation is that our measurements were from whole-cell lysates, not nuclear fractions. Although HO-1 upregulation suggests pathway activation, we cannot conclusively confirm ISRIB promoted Nrf2 nuclear translocation. Future studies employing nuclear fractionation or immunofluorescence are needed to definitively confirm this. Additionally, quantifying phosphorylated PERK (p-PERK) would directly link HG stress to PERK activation and strengthen mechanistic insights, representing an important focus for future research.

Mechanistically, HG induces ferroptotic priming via lipid peroxidation surge consistent with GPX4 depletion [35] and lysosomal iron catalysis [36]. ISRIB's concurrent attenuation of apoptosis and pyroptosis suggests that mitochondrial pore formation via VDAC oligomerization, facilitating co-release of apoptogenic and inflammatory factors [37, 38], may represent a key convergence point. The PERK-GSDMD axis linking ER stress to pyroptosis [39] also warrants further investigation in this context.

Despite these nuances, our findings have significant therapeutic implications. ISRIB's ability to rescue cell viability by simultaneously targeting three distinct death pathways suggests that modulating the ISR may offer advantages over monospecific inhibitors. This multi-pathway suppression is critical for preserving the retinal vasculature in diabetes, where metabolic memory [40] and

oxidative/hemodynamic interplay [41] complicate treatment. ISRIB's favorable ocular pharmacokinetics [42] and absence of toxicity under normoglycemia in our study address translational concerns. Furthermore, our proteomic data indicating VEGF receptor 2 downregulation hint at synergy with existing anti-angiogenic therapies [43], while PPARγ agonists, known to protect via crosstalk with Nrf2 [44, 45], may complement this approach.

In conclusion, we redefine HG-induced endothelial injury in DR as a convergent process of ferroptosis, apoptosis, and pyroptosis driven by ER stress and lipid metabolic shifts [46]. Targeting the ISR with ISRIB to activate the Nrf2/HO-1 axis offers a promising integrated therapeutic strategy. Future studies should include p-PERK detection and Nrf2 nuclear translocation assays to solidify mechanistic links, utilize diabetic Perk haploinsufficient models [47] to isolate PERK's role, explore PPAR-Nrf2 pathway crosstalk, and optimize nanoparticle-based intraocular delivery [48] to advance clinical translation.

5 Conclusion

This study demonstrates that HG triggers a convergent network of ferroptosis, apoptosis, and pyroptosis in HRECs. We identify pharmacological modulation of the ISR using ISRIB as a potent strategy to simultaneously suppress these cell death pathways, mechanistically linked to restoration of the Nrf2/HO-1 antioxidant axis. These findings redefine early DR pathogenesis as a PERK-regulated triad of cell death, positioning ISR inhibition as a promising integrated therapeutic approach. Future studies are needed to validate this axis in vivo and to optimize intraocular delivery of ISRIB, advancing the translation of this protective strategy toward clinical preservation of the diabetic retina.

Funding Declaration

This work was supported by the Sichuan Provincial Department of Science and Technology (No.2024ZYD0114) ,Sichuan Medical Association (No. S2024001) and Sichuan Association of Integrated Traditional Chinese and Western Medicine (No.ZXY2025017).

Author contributions

Like Xie: Writing,-original draft, Software, Methodology, Formal analysis,Conceptualization.Xinarn Zhang:Software,Methodology,Formalanalysis.Min Tian:Software, Methodology, Formal analysis. Min Tang:Investigation.Software, Methodology. Qi Zhou:Supervision Project administration. Hongbin Lv: Supervision Project administration, Fundingacquisition, Conceptualization.

Data availability

The primary data of this study can be obtained from the corresponding author uponreasonable request.

Declarations

The authors declare no conflict of interestFootnotes

Publisher's Note

Springer Nature remains neutral with regard to jurisdictional claims in publishedmaps and institutional affiliations

Like Xie and Xinran Zhang contributed equally to this work.

Contributor Information

Like Xie,Email: 409035642@qq.com.

Affiliated Hospital of Southwest Medical University, Luzhou, China

Xinran Zhang,Email: 910943955@qq.com.

Affiliated Hospital of Southwest Medical University, Luzhou, China

Min Tian, Email: 181755721@qq.com.

Affiliated Hospital of Southwest Medical University, Luzhou,

China

Min Tang,Email: tangmin1828@163.com.

Affiliated Hospital of Southwest Medical University, Luzhou, China

Qi Zhou,Email: 113454771@qq.com.

Affiliated Hospital of Southwest Medical University, Luzhou, China

Hongbin Lv, Email: oculistlvhongbin@swmu.edu.cn.

Affiliated Hospital of Southwest Medical University, Luzhou, China

6 Reference

1. Teo ZL, Sabanayagam C, Cheung G, et al. Global prevalence of diabetic retinopathy and projection of burden through 2045: systematic review and meta-analysis Prog Retin Eye Res. 2021;83:100919.
2. Antonetti DA, Klein R, Gardner TW. Diabetic retinopathy. N Engl J Med. 2012;366(13):1227-1239.
3. Simó R, Hernández C. Neurodegeneration in diabetic retinopathy: does it really matter? Lancet Diabetes Endocrinol. 2016;4(4):345-356.
4. Kowluru RA, Mishra M. Mitochondrial stability in diabetic retinopathy: lessons learned from epigenetics. Biomedicines. 2021;9(8):918.
5. Li J, Cao F, Yin H, et al. Ferroptosis: past, present and future. Cell Death Dis. 2020;11(10):838.
6. Zhang Z, Guo M, Li Y, et al. Endothelial cell ferroptosis mediates monocrotaline-induced pulmonary hypertension. Redox Biol. 2022;51:102279.
7. Tang M, Chen Z, Wu D, et al. Ferroptosis: new insights into the mechanisms of diabetic complications. Diabetes Metab J. 2023;47(1):38-52.
8. Chen Y, Brandizzi F. PERK-dependent activation of Nrf2 contributes to redox homeostasis and cell survival following endoplasmic reticulum stress. Cell Death Differ. 2014;21(3):377-389.
9. Wang J, Zhu P, Toan S, et al. Pumilio2 protects against diabetic cardiomyopathy by suppressing PERK-mediated ER stress. Diabetologia. 2017;60(6):1059-1071.

10. Zhong Y, Wang J, Yang S, et al. Targeting ER stress alleviates high glucose-induced endothelial dysfunction. Diabetes. 2022;71(8):1721-1734.
11. Xue M, Qian Q, Adaikalakoteswari A, et al. Activation of NF-E2-related factor-2 reverses biochemical dysfunction of endothelial cells induced by hyperglycemia. Diabetes. 2008;57(10):2809-2817.
12. Jiang T, Tian F, Zheng H, et al. The protective role of Nrf2 in streptozotocin-induced diabetic nephropathy. Oxid Med Cell Longev. 2021;2021:8875726.
13. Yang M, Wang L, Wang X, et al. Nrf2 activation rescues hyperglycemia-induced endothelial dysfunction. Biochim Biophys Acta Mol Basis Dis. 2023;1869(1):166582.
14. Gandhi NK, Kapoor R, Stevens T, et al. Proteomic analysis of retinal mitochondria identifies oxidative stress responses in early diabetic retinopathy. J Proteome Res. 2011;10(2):492-506.
15. Liu X, Zhang J, Guo X, et al. PPARγ prevents hyperglycemia-induced endothelial dysfunction by inhibiting ROS generation. Mol Med Rep. 2020;21(1):309-317.
16. Shi R, Zhao L, Wang F, et al. TMT proteomics analysis of retinal endothelial cells under high glucose. Exp Eye Res. 2022;215:108914.
17. Dixon SJ, Lemberg KM, Lamprecht MR, et al. Ferroptosis: an iron-dependent form of nonapoptotic cell death. Cell. 2012;149(5):1060-1072.
18. Tang D, Kang R, Berghe TV, et al. The molecular machinery of regulated cell death. Cell Res. 2019;29(5):347-364.
19. Wang Y, Gao W, Shi X, et al. Chemotherapy drugs induce pyroptosis through caspase-3 cleavage of gasdermin E. Nature. 2017;547(7661):99-103.
20. Oshitari T, Roy S. Endoplasmic reticulum stress and diabetic retinopathy. Int J Mol Sci. 2021;22(9):4256.
21. Li W, Pang Y, He H, et al. High glucose induces mitochondrial dysfunction in retinal endothelial cells. Invest Ophthalmol Vis Sci. 2022;63(13):16.
22. Joussen AM, Poulaki V, Le ML, et al. A central role for inflammation in the pathogenesis of diabetic retinopathy. FASEB J. 2004;18(12):1450-1452.
23. Chen L, Yang G, Zhang X, et al. PERK/Nrf2 pathway activation protects against ferroptosis in diabetes. Front Cell Dev Biol. 2021;9:651317.
24. Sidrauski C, Acosta-Alvear D, Khoutorsky A, et al. Pharmacological dimerization and activation of the exchange factor

eIF2B antagonizes the integrated stress response. eLife. 2015;4:e05098.
25. Zhang K, Han X, Yang M, et al. Lipid remodeling in diabetic complications revealed by mass spectrometry. Nat Metab. 2022;4(5):626-642.
26. Li F, Zhang Z, Wang Y, et al. Molecular mechanisms and disease implications of ferroptosis. Acta Pharm Sin B. 2023;13(1):1-28.
27. Kanehisa, M., Sato, Y., Kawashima, M., Furumichi, M., and Tanabe, M.; KEGG as a reference resource for gene and protein annotation. Nucleic Acids Res. 44, D457-D462 (2016).
28. Kanehisa, M. and Goto, S.,: KEGG: Kyoto Encyclopedia of Genes and Genomes. Nucleic Acids Res. 28, 27-30 (2000).
29. Zhu M, Wang L, Liu R, et al. Proteomic signature of ferroptosis in diabetic retinopathy. Exp Eye Res. 2023;227:109381.
30. Gao M, Yi J, Zhu J, et al. Mitochondrial fission drives ferroptosis through iron-dependent lipid peroxidation. Nat Commun. 2023;14(1):3123.
31. Bai J, Liu F, Nie S, et al. Mitochondrial DNA release activates cGAS-STING in hyperglycemia. Nat Immunol. 2021;22(10):1268-1279.
32. Wang C, Xu S, Liu Y, et al. cGAS-STING pathway mediates inflammation in diabetic vasculopathy. Nat Commun. 2023;14(1):2122.
33. Chen X, Li P, Wu Z, et al. PERK directly phosphorylates Nrf2 to repress antioxidant response in endothelia. Redox Biol. 2023;60:102612.
34. Liu R, Chen Y, Zhang Y, et al. Neuron-specific PERK activation of Nrf2 under oxidative stress. Neuron. 2022;110(21):3596-3613.
35. Yang L, Wang F, Zhang G, et al. GPX4 degradation and SLC7A11 suppression drive ferroptosis in hepatocytes. Hepatology. 2023;77(1):223-239.
36. Huang Y, Xu M, Liu J, et al. Lysosomal iron catalyzes lipid peroxidation in ferroptosis. Cell Metab. 2023;35(1):1-18.
37. Chen J, Zhang K, Liu M, et al. VDAC oligomerization enables mitochondrial co-release of cytochrome c and IL-1β. Sci Adv. 2023;9(15):eadf3978.
38. Deng F, Yang Q, Li R, et al. Targeting mitochondrial pores in septic shock. Sci Transl Med. 2022;14(667):eabq6293.
39. Xu S, Wu H, Lu X, et al. PERK-GSDMD axis links ER stress to pyroptosis. Cell Rep. 2022;41(7):111630.
40. Kowluru RA, Kowluru A, Mishra M. Metabolic memory in diabetic complications. Metabolites. 2023;13(2):193.

41. Hammes HP, Feng Y, Pfister F, et al. Oxidative stress and hemodynamic forces in diabetic retinopathy. Diabetologia. 2021;64(7):1505-1521.
42. Jiang Y, Zhang P, Xu R, et al. Ocular delivery of ISRIB using thermosensitive hydrogel. J Control Release. 2022;348:796-808.
43. Chatziralli I, Theodossiadis G, Dimitriou E, et al. Combination therapies with anti-VEGF agents in diabetic retinopathy. Ophthalmol Ther. 2023;12(1):141-156.
44. Li X, Zhao M, Chen L, et al. PPARγ agonists protect retinal endothelial function. Diabetes Care. 2023;46(1):dc220863.
45. Liu X, Zhang J, Guo X, et al. PPARγ-Nrf2 crosstalk in endothelial protection. Mol Med Rep. 2020;21(1):309-317.
46. Santos CX, Nabeebaccus AA, Shah AM, et al. Endoplasmic reticulum stress and lipid metabolism in diabetes. Nat Commun. 2022;13(1):5114.
47. Song X, Wang J, Liu K, et al. Perk^{+/-} mice show attenuated diabetic retinopathy. JCI Insight. 2022;7(10):e158468.
48. Zhu M, Wei Y, Xu H, et al. Nanoparticle strategies for ocular drug delivery. Adv Drug Deliv Rev. 2023;192:114642.

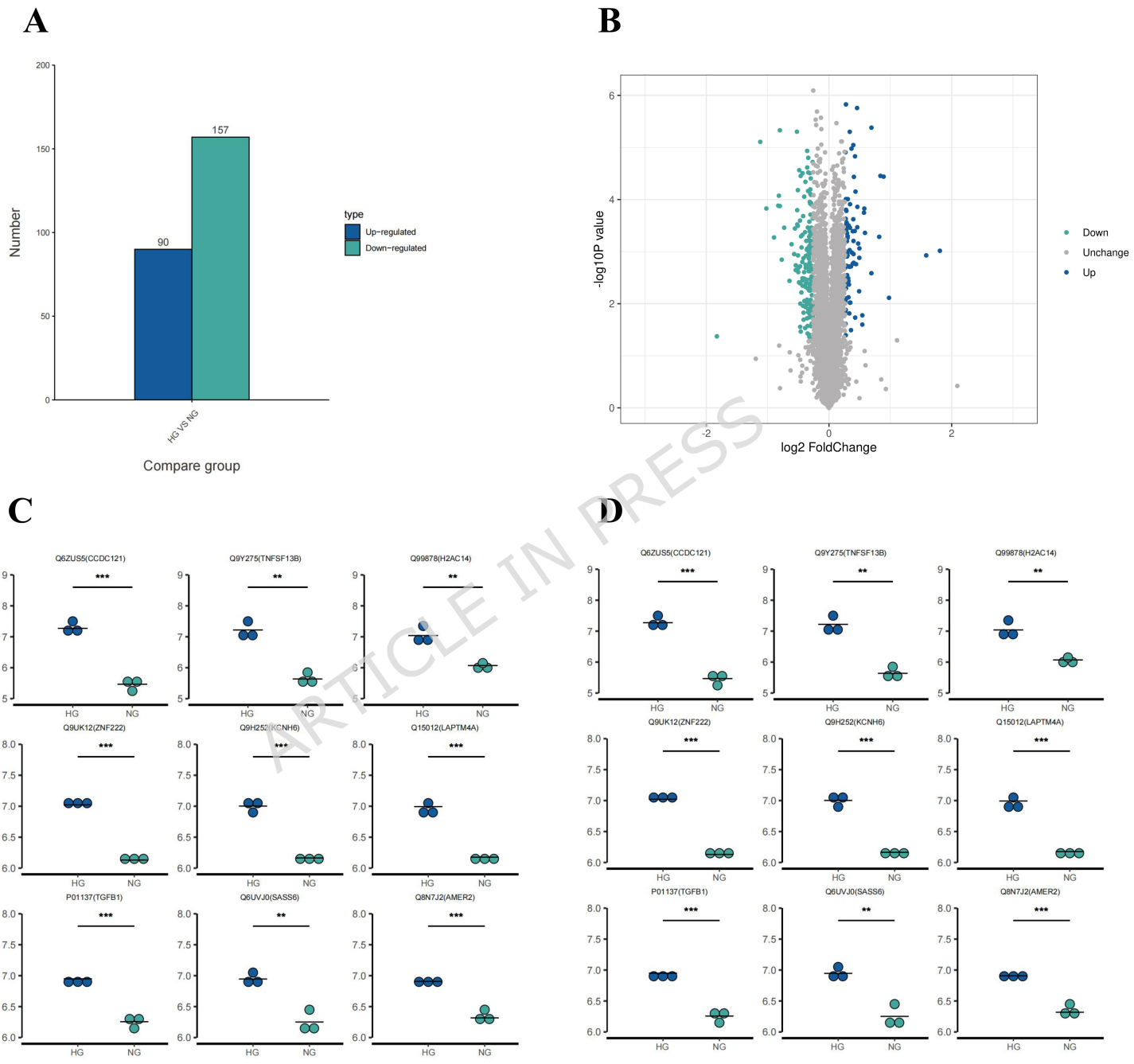

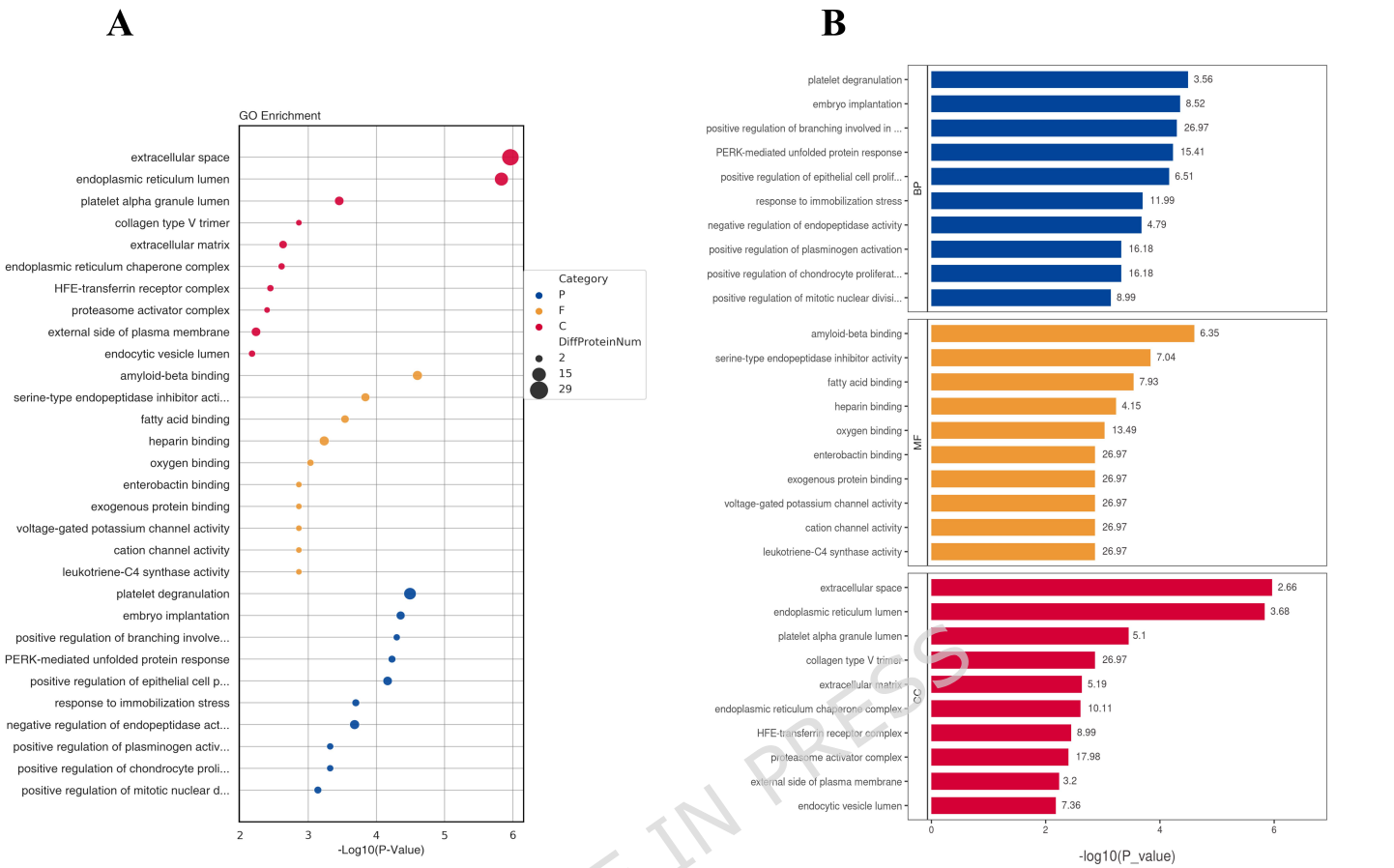

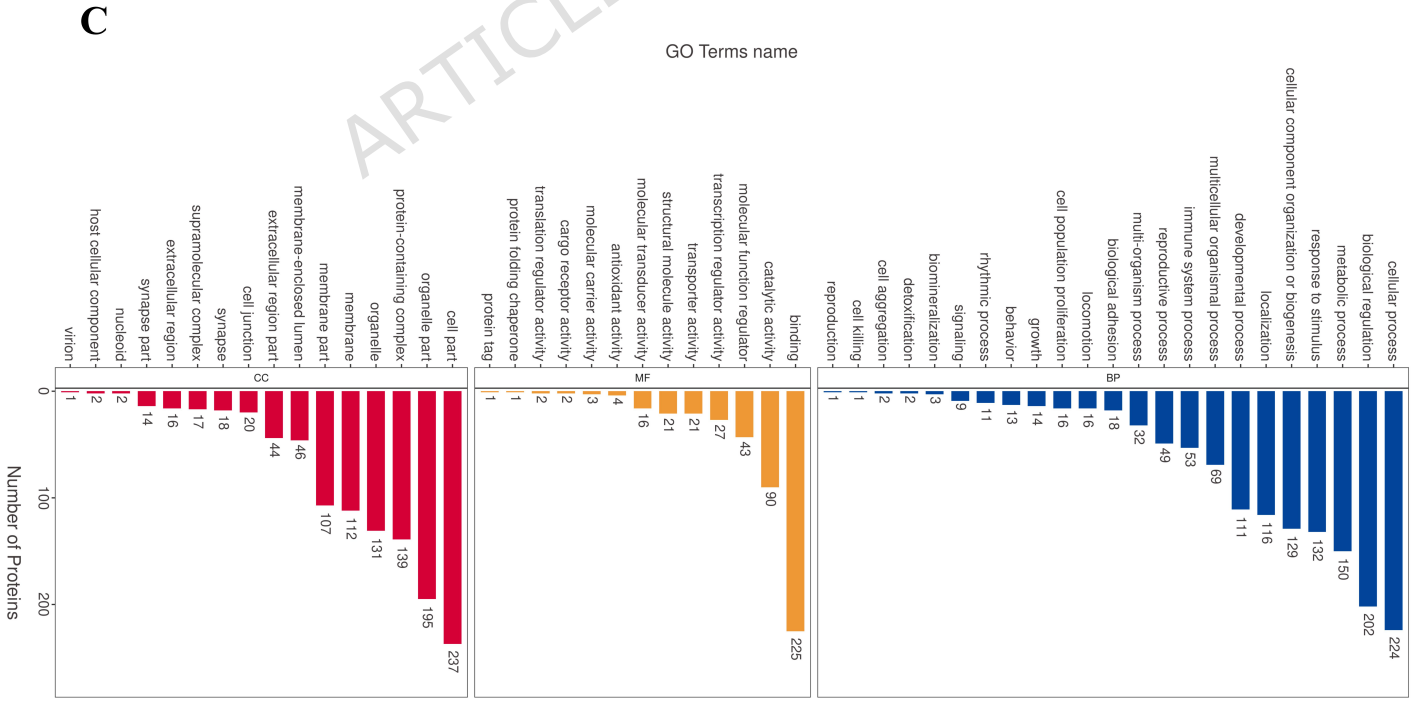

A

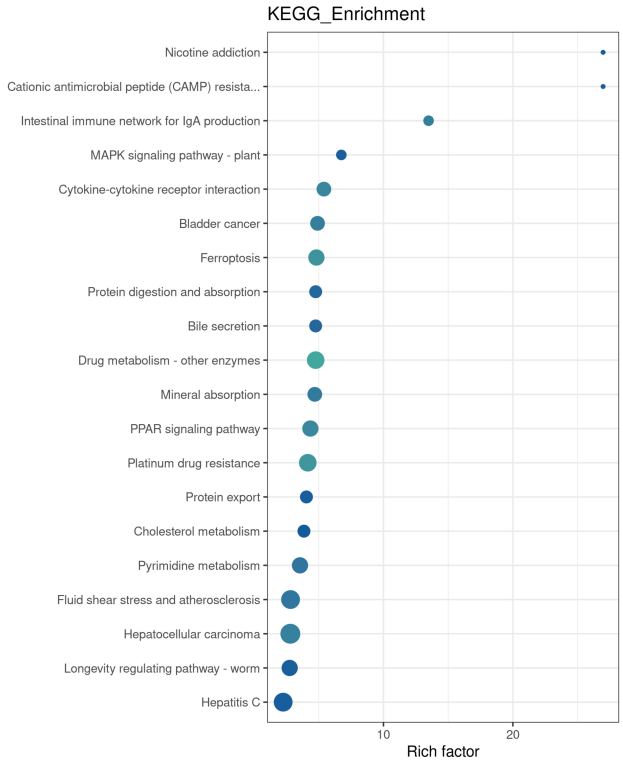

B

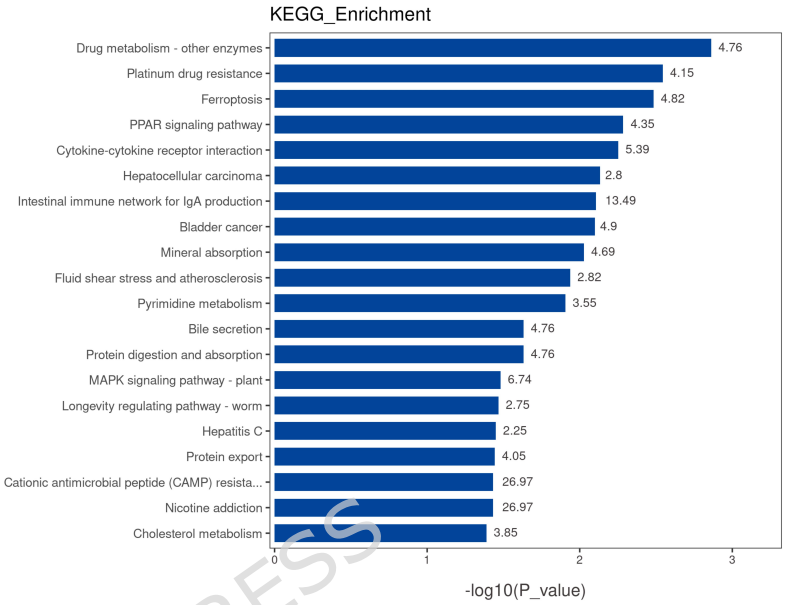

C

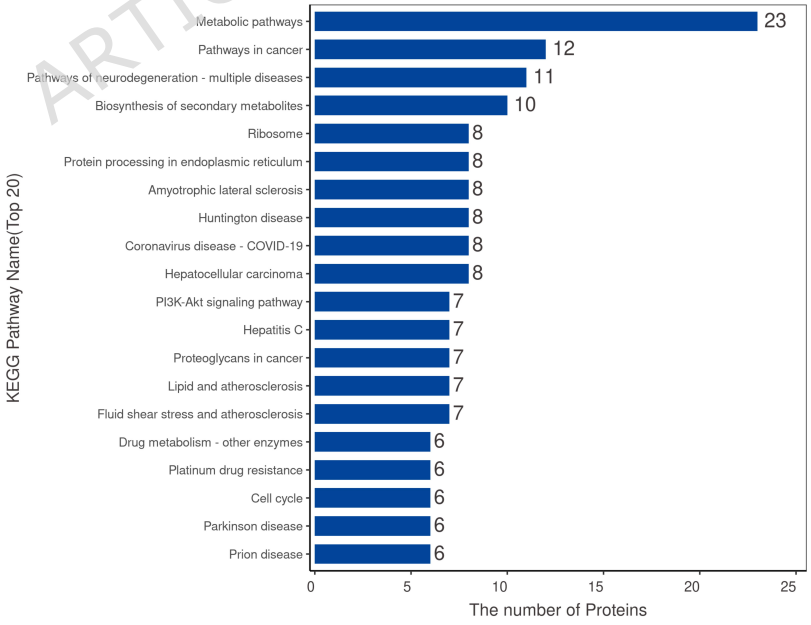

A

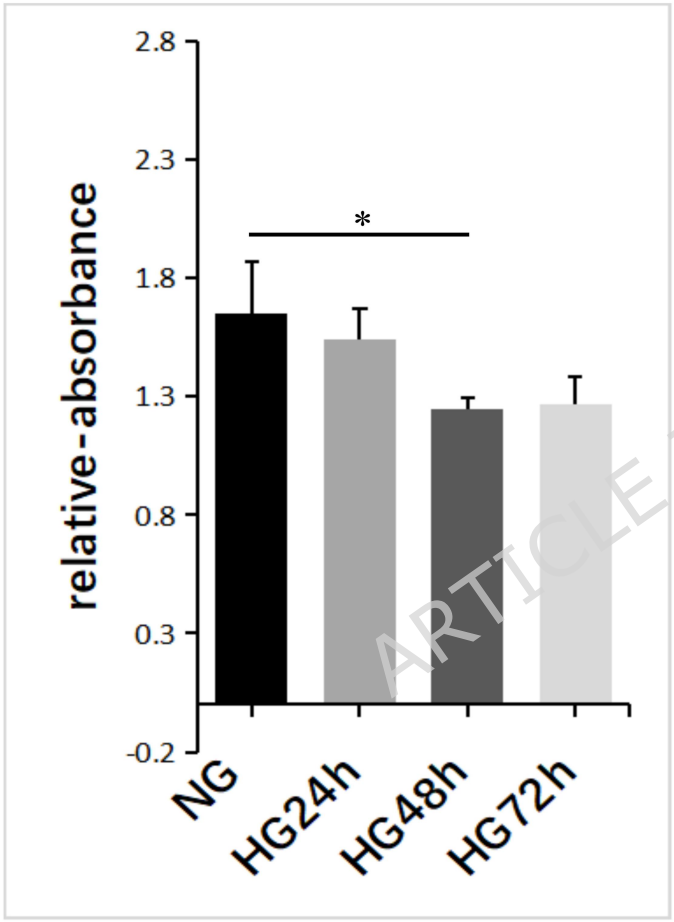

B